Design and Construction of a Sensor to Monitor Blood Parameters During Resuscitation

Nathaniel Coulson

A dissertation

submitted in partial fulfillment of the

requirements for the degree of

Master of Science in Bioengineering

University of Washington

2015

Committee:

Pierre D. Mourad, Ph.D.

Christopher Neils, Ph.D.

Program Authorized to Offer Degree:

Bioengineering

University of Washington

Abstract

Design and Construction of a Sensor to Monitor Blood Parameters during Resuscitation

Nathaniel Coulson

Chair of the Supervisory Committee:

Pierre D. Mourad, Ph.D., Associate Professor

Neurosurgery.

When performed by professional medical staff, cardiopulimary resuscitation (CPR) is successful in resuscitating patients in less than 45% of cases. Even in cases where patients survive, brain damage due to partially hypoxic conditions is a significant cause of morbidity. Monitoring cerebral oxygenation during resuscitative procedures has the potential to improve effectiveness by providing real time feedback for attending medical personnel. This will enable quick and informed procedural alterations, especially when conditions do not allow use of the full breadth of medical technology. We present work towards a device capable of providing real time information concerning the cerebral oxygenation and perfusion of a patient. We have considered both direct monitoring of cerebral oxygenation and perfusion using a transcranial ultrasound/NIRS system and ultrasound based monitoring of carotid blood flow as a proxy for cerebral oxygenation and perfusion. Two studies were performed in a poly-trauma pig model to test the viability of carotid based blood flow monitoring during critical conditions. In both cases, blood flow was detectable until near death conditions at mean arterial pressures (MAP) as low as 28 mmHg. Additionally, heart rate was accurately measured across all experimental conditions. As a result of positive initial data, a custom transducer was designed to carry this project further into pig studies and eventually human based research studies.

Background

There are over 500,000 instances of cardiac arrest every year in the United States, with less than 50% occurring in a hospital setting [1]. Even with advanced care readily available, the adult in-hospital survival rate is below 25% [1]. If cardiac arrest occurs outside of the hospital environment, the survival rate is significantly lower at 9.5%. Even patients whose heart is restarted often experience rates of morbidity or mortality as high as 70% due to the effects of post-cardiac arrest syndrome (PCAS) [2]. Post-cardiac arrest syndrome is a result of a combination of issues associated with heart attack including brain injury, myocardial dysfunction, and issues related to systemic ischemia/reperfusion response [2]. Of interest in this work is post-cardiac arrest brain injury. During an ischemic attack or periods without a pulse, circulation to the brain is heavily compromised, causing hypoxic conditions for neurological tissue. Due to high metabolic demands, brain chemistry begins to change within seconds of the onset of hypoxic conditions and cell death can begin to occur in as little as 5 minutes with inadequate oxygen supply [3]. While the primary medical goal must be to restart or restore function to the heart, post-cardiac arrest brain injury represents a significant secondary issue that may be at least partially addressed by tailoring resuscitation techniques to increase cerebral blood flow. Recent adaptations in cardio-pulmonary resuscitation (CPR) techniques suggest that out-of-hospital cardiac arrest survival may be significantly increased by administering chest compression only CPR [4]. This modified CPR, Cardiocerebral Resuscitation, focuses on delivering the maximum amount of blood to the brain during resuscitation. While this simple procedural change may result in reduced mortality, no technology currently exists to monitor cerebral blood parameters during resuscitative measures. Information about blood flow to the brain or saturated peripheral oxygen (SpO_2) during this critical time would give attending personnel feedback that is paramount to preventing long term neurological damage or brain death. A real time monitoring device would allow procedural changes to resuscitation techniques on the fly and possibly facilitate the development of new resuscitation procedures.

Brain Oxygen and Perfusion Monitoring

Introduction

The ideal solution for a real time cerebral oxygenation and blood flow monitoring device would be to directly measure blood oxygen levels (SpO_2) and blood perfusion, from a non-invasive package. Direct monitoring would provide attending personnel with the most useful information to assist in altering their resuscitation procedures. Pulse oximetry products are readily available for monitoring SpO_2 in locations through which some light can pass, like the fingertip. Devices that measure blood oxygen saturation in deep tissue or through bone are limited by photon penetration through tissue. Near infrared spectroscopy (NIRS) partially

addresses this issue as devices based in this range may penetrate several centimeters into tissue [5]. While care can be taken to minimize the effect of extracerbral tissue on NIRS measurements by placing the transmitter and receiver farther apart, it cannot be eliminated. Increasing separation increases mean depth of penetration, but cannot eliminate signal from superficial tissue [6]. Significant attenuation also occurs through superficial tissue and bone, resulting in a diminished signal to noise ratio even near maximum safe power. Several technologies exist on the market leveraging NIRS for non-invasive cerebral blood oxygenation monitoring, including the INVOS™ system from Medtronic. While the majority of these systems are clinically validated, they may be prohibitively expensive for many locations and are not readily portable, making them less available for resuscitation situations.

Xu et al. have proposed an ultrasound based mechanism that has the potential to overcome some of the difficulties associated with transcranial NIRS [7]. Their work suggests the ability to tag photons in a scattering medium using ultrasound to locally induce a Doppler shift. Detected photons from the area being exposed to ultrasound could then be differentiated from other multiply scattered photons. This technology has the potential to enable local blood oxygenation measurements transcranially, ignoring signal from unwanted extracranial tissue components.

We propose combining these technologies with transcranial Doppler ultrasound, which has been repeatedly demonstrated to give a reliable assessment of cerebral profusion, to develop portable system capable of monitoring cerebral oxygenation and perfusion during resuscitation [8]. A portion of my research focused on the development of an initial prototype device through proof of concept experimentation. This development was broken in to three phases. First, demonstrate ultrasound can induce a Doppler shift in laser light by focally vibrating tissue. Next, design and test the only the ultrasound components of the system. This includes focal tissue vibration and perfusion monitoring using a transcranial Doppler system. Last, incorporate and test a two wavelength laser light system capable of detecting blood oxygen saturation. Due to a combination of factors that culminated in the postponement of this project, only step one was addressed in this research. This is expanded up in the discussion for this section.

Experimental Setup and Methods

Laser Doppler System

In order to measure blood oxygenation saturation (SPO_2) co-locally with a focused ultrasound source, it was necessary to first prove that our focused ultrasound source could generate tissue vibration to induce a photon Doppler shift. A TSI Powersight laser Doppler velocimetry (LDV) system was employed in conjunction with our ultrasound source to measure particle

movement within a tissue mimicking substance (TSI Inc., Shoreview MN). This setup used a Melles Griot 543 series argon ion laser to generate multicolor laser light (Melles Griot, Rochester NY). The laser is passed through a TSI Fiberlight multicolor beam separator to create a pair of blue 488 nm and a pair of green 514.5 nm beams. One of each beam, blue and green, are shifted by 40 MHz using a built in Bragg cell. All four beams were optically focused by to converge at a distance of 50 cm from the lens. Light was collected from the focal region using a TSI RV 70 phase Doppler receiver and amplified with a TSI PDM 100 photo detector module. Amplified light was digitized using and TSI FSA 4000 multibit digital processor and analyzed using TSI's Flowsizer software. This system creates a fringe pattern at the intersection of the laser beams. Particles moving through this fringe pattern, perpendicular to the incident laser, can be detected by the difference in reflected light in the illuminated and dark fringes. The 488nm blue beams measure velocity in x, while the 514.5nm green beams measure velocity in y (Figure 1).

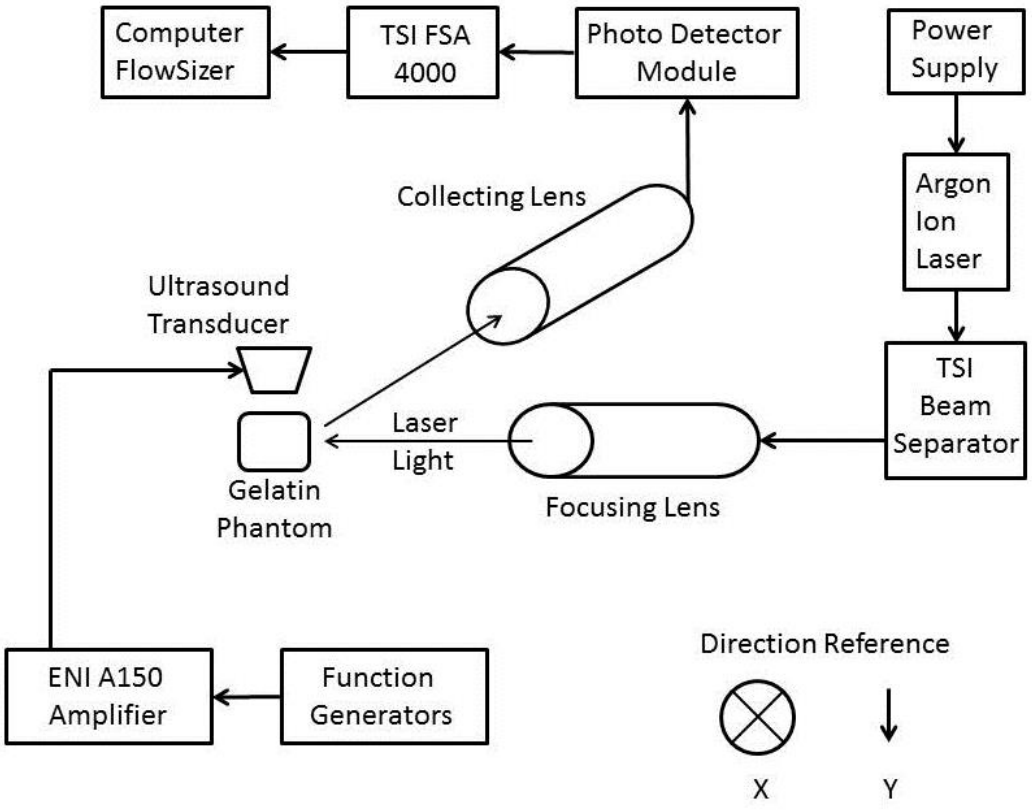

Figure 1 – Experimental setup for measuring ultrasound induced motion in a tissue mimicking phantom. The ultrasound transducer was secured to 2D motion stage to allow translation across the top of the phantom.

Ultrasound Delivery System

Focused ultrasound was produced using a custom built, single element, concave 1.1 MHz transducer with a focal distance of 63mm. A machined plastic cone 40mm in length was placed on the transducer to position the device to be farther away from the sample and to enable easier coupling. This resulted in the focal region 23mm from the face of the cone. The cone volume was filled with deionized, degassed water and a layer of latex was secured over the cone to keep the water in place. The transducer assembly was coupled to the tissue mimicking gel phantom using standard ultrasound coupling gel. The LDV system is designed to detect velocity in the planes perpendicular to the direction of laser propagation. The ultrasound was aligned in the x-y plane perpendicular to the laser to create detectable oscillations in the tissue mimicking phantom (Figure 1).

Ultrasound signals were generated using two function generators in a gated setup. The gating function generator was an Agilent 33250A (Agilent Technologies, Santa Clara CA) and the driving function generator was a Hewlett Packard 33120A (Hewlett-Packard, Palo Alto CA). A LeCroy Waverunner LT322 oscilloscope was used to monitor the signal bursts and ensure proper configuration (Teledyne, Thousand Oaks CA). Output signals were amplified using an ENI A150, 150 Watt amplifier to achieve sufficient output pressure (ENI, Rochester New York).

Phantom Design and Construction

Initial phantoms were constructed using Jeltrate alginate. Alginate is a cold setting gel that allows quick phantom construction with similar acoustic properties to tissue [9]. It cures quickly (~30 min) and can be cut after curing to create a wide variety shapes that do not require a custom mold. Phantoms were later comprised of gelatin, which cures clear, to increase laser penetration and signal strength. To maintain the gelatin clarity, standard scattering and sound speed adjusting additives were omitted; however, gel properties remained sufficiently close to tissue for initial experimentation [10]. Preparation of both materials is outlined below.

Alginate phantoms were prepared using Jeltrate alginate and ultrapure deionized/degassed water. Water was added to a standard kitchen blender for mixing. 4% by mass alginate powder was added in small portions to avoid any clumping and ensure homogeneity and mixed on a low setting. 140mg of simethicone were added to disrupt bubble formation. Immediately after mixing, the alginate solution was poured into a rectangular glass container that served as a mold and placed in a vacuum degassing chamber for 4 minutes to remove trapped air. Air was reintroduced into the vacuum space slowly over 30 seconds to prevent surface disruption of the phantom and unnecessary bubble formation. Once removed, a 1 cm in diameter metal bar was placed into the phantom to create a cavity and held in place using a standard ring stand. The cavity was situated as close to the optically incident edge of the phantom as possible to

minimize the distance the laser must travel. After curing for 15 minutes the phantom was sufficiently solid to allow removal of the bar, leaving a cylindrical cavity in the phantom. 20 mL of additional alginate solution was prepared as above and .1-2% by mass 400 grit (22 um particle size) aluminum oxide powder was added during mixing. The Al_2O_3 acted as a scattering agent for the laser light enabling the LDV system to track particulate motion. The phantom was then allowed to cure fully (30 minutes) and was covered with degassed water and parafilm to prevent evaporation. The phantom was cut using a thin, very taut wire to position the ultrasound contact region 23mm from Al2O3 scattering zone (Figure 2).

Gelatin phantoms were prepared using 300-Bloom gelatin derived from acid-cured porcine skin (Sigma-Aldrich Corp., St. Louis MO) and ultrapure deionized/degassed water as suggested by Cook et al. [10]. The water was added to a beaker, covered with parafilm to prevent excess evaporation, and heated to 30° C. The solution was stirred vigorously using a magnetic stir bar and 4% gelatin powder by mass was added slowly to prevent aggregation. The solution was heated to 45°C over 10 minutes and stirred until completely dissolved. The gelatin was placed in a vacuum degassing chamber for 10 minutes to remove any introduced air. After degassing, the material was poured into the glass mold, and placed in a 4 degree C fridge for 24 hours to allow the cross-linking process to complete. A cavity was created in the same manner described above. 20 mL of additional gelatin was prepared using the above process and .1-2% Al_2O_3 was added during mixing and heating. After degassing, this solution was gently stirred a final time using a glass rod to prevent sedimentation of the Al2O3 and was poured into the void. The phantom was again covered in parafilm and placed in the fridge for 24 hours to allow cross-linking to fully occur. The phantom was cut as described above (Figure 2).

LDV Measurements

The phantom was situated in the path of the laser such that the intersection of the 4 beams lay just inside the Al_2O_3 scattering region of the phantom. The ultrasound transducer assembly was secured to a 2D motion stage and placed against the phantom such that the ultrasound and laser systems were confocal. The ultrasound was aligned in the y direction, parallel to the 514.5nm beams in order to induce tissue movement in a single direction.

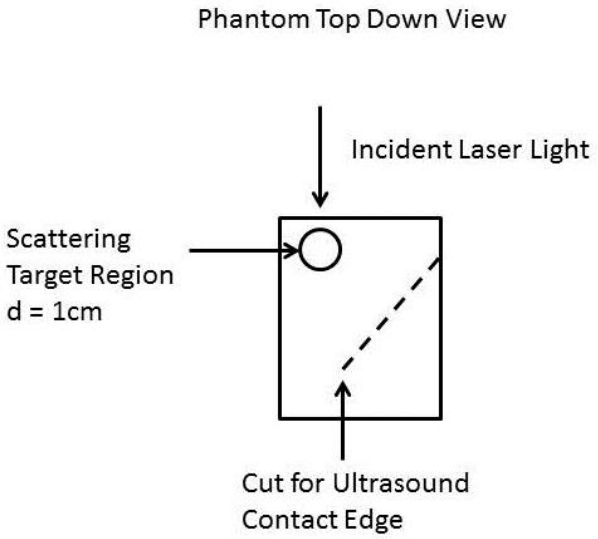

Figure 2 – Schematic of the phantom construction. The angle at which the gel was cut varied, but the distance from the cut to the scattering region was always 23 mm. The scattering region was placed within 2 mm of the incident laser edge.

Bandpass Frequency Range	Mininum Measurable Velocity m/s	Maximum Measurable Velocity m/s
.3-3 kHz	0.0012	0.012
1-10 kHz	0.004	0.04
3-30 kHz	0.012	0.12
10-100 kHz	0.04	0.4
30-300 kHz	0.12	1.2
100-1000 kHz	0.4	4
.3-3 MHz	1.2	12
1-10 MHz	4	40
2-20 MHz	8	80
5-30 MHz	20	120

Table 1 – A list of bandpass filters built into FlowSizer that were attempted. The minimum and maximum detectable velocity for each range is also displayed.

The user controlled bandpass filter, which allows detection of different Doppler frequency ranges, was initially set at its minimum value, .3-3 kHz. Due to of the 40 MHz Bragg cell, the system detects frequencies 40 MHz + the Doppler frequency f_d. Depending on the direction of travel, f_d may be positive or negative. As a result, the signal downshift was set to the center of the current bandpass range to allow detection of bi-directional motion. During testing with ultrasound, each sequential bandpass filter was selected to test for ultrasound induced motion. Table 1 shows each attempted bandpass filter and its maximum and minimum detectable particle velocities. Photomultiplier tube voltages were set as high as possible to provide adequate amplification of low signal strength. The reason for this is expanded upon in the discussion. Data was collected for no less than 60 seconds. It was often necessary to let data collection run for 2-4 minutes to get any recordable signal.

Ultrasound was applied in bursts to the phantom material in order to generate vibration using radiation force pressure (RFP). By pulsing ultrasound at regular intervals, the tissue is subjected to cycles of ambient and greater than ambient pressure, causing vibration. On each phantom a combination of powers, pulse durations, and pulse repetition frequencies (PRF) were used. Applied voltage (pressure) and pulse duration were initially set very low and increased incrementally if no signal was detected. Applied voltage from the function generator ranged from 50 to 350 mV_{pp} corresponding to output pressures of 151.5 kPa to 6.06 MPa. Pulse duration varied from 50 to 3000 µs and PRF was calculated from the desired pulse duration to give a 50% duty cycle. Applied voltage from the function generator was capped at 350 mV, 225 V_{pp} to the transducer after amplification, to prevent any damage to the transducer element.

Results

In order to collect data, the LDV system must receive some minimum amount of useful photons. In addition, the Doppler frequency waveform detected by the system must be of sufficient quality for a velocity to be calculated. If these conditions are not met, the systems data rate will be zero and no velocity information can be measured. This led to significant difficulty in setting up the system to collect any data at all. In most instances, regardless of the steps taken maximize the laser signal, no data could be obtained. In the vast majority of cases where data any could be collected, only sporadic noise could be recorded. Figure 3 shows examples of data collected in a gelatin phantom without ultrasound present using 1% Al_2O_3 by mass in the scattering region that are suspected to be noise. Data in green represents vertical velocity in y and data in blue represents horizontal velocity in x (see Figure 1). Ultrasound was applied in the vertical (y) direction. Figure 4 shows data collected from the same phantom during ultrasound administration. In this case output pressure was 6.06 MPa and pulse duration was 1000 µs. Data was collected for more than 60 seconds.

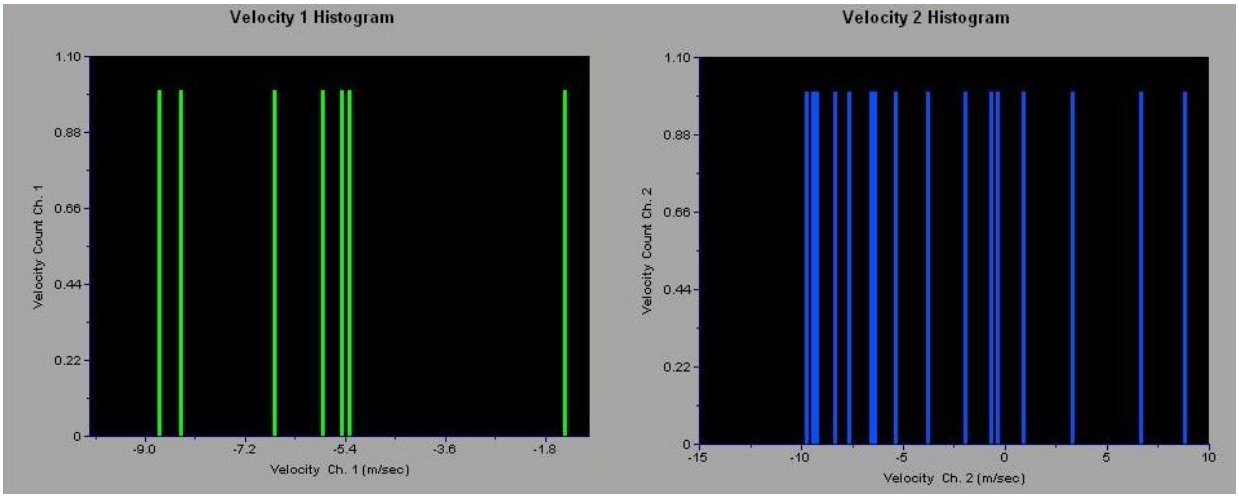

Figure 3 – Examples of data collected from a phantom during application of ultrasound where only noise was visible. This was the primary form of data collected. The graph in green (left) represents vertical velocity in y. The graph in blue (right) shows horizontal velocity in x.

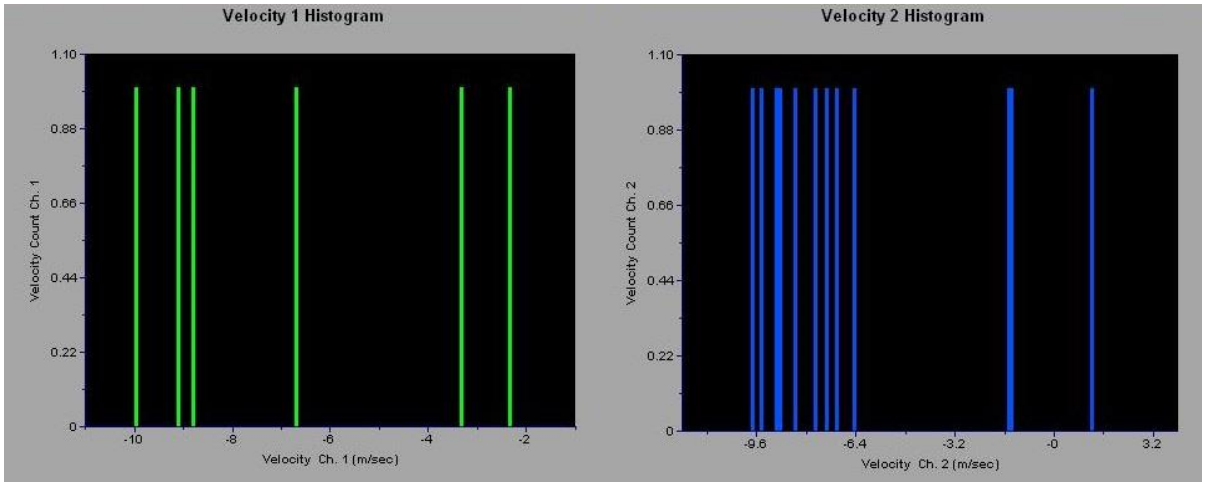

Figure 4 - Examples of data collected from a phantom without application of ultrasound where only noise was visible. The graph in green (left) represents vertical velocity in y. The graph in blue (right) shows horizontal velocity in x.

We suspect Figures 3 and 4 are only recording noise for several reasons. First each bar corresponds to only a single calculated velocity, where a distribution with hundreds of counts is expected. Additionally there is no discernable difference between velocity in the direction of ultrasound propagation (green) between Figures 3 and 4. Velocities in x show some difference between ultrasound on and off but too few points are collected to make any inference. To confirm that this was indeed only spurious noise being collected, a humidifier was substituted for the phantom and the system was allowed to collect data from moving water droplets in air. Immediately upon substitution, data was readily available. Figure 5 is an example of the x velocity distribution recorded from the humidifier aimed horizontally in x. The number of data points acquired when the system is measuring properly is much higher, with many samples per bin. Additionally, there is a velocity shift in humidifier data, with the mean velocity around .4 m/s. No shift was ever discernable in phantom data.

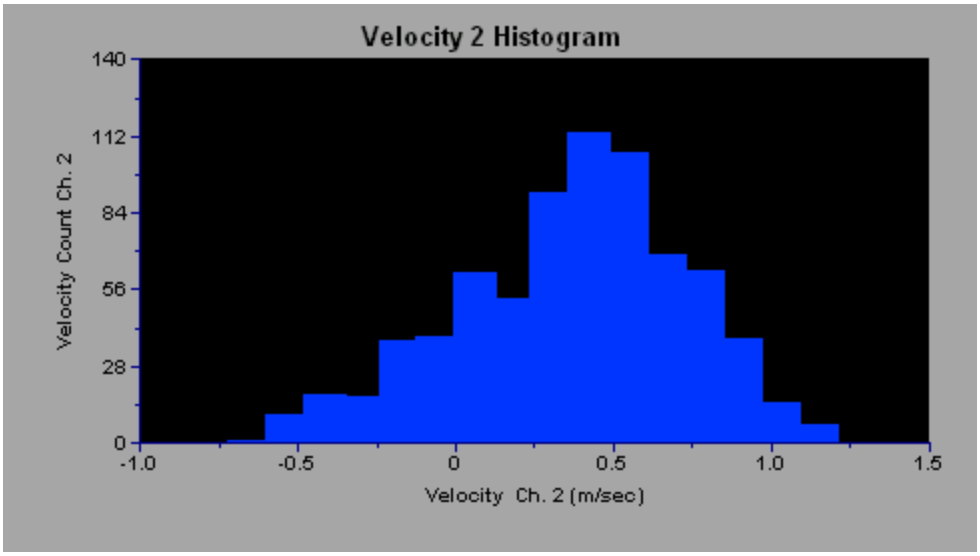

Figure 5 - Data collected from water vapor particles generated using a humidifier. There is a discernable shift in the mean velocity to approximately .4 m/s.

In a handful of runs, data could be collected when the gel was present. Figure 6 shows data from a gelatin phantom without ultrasound application. Figure 7 shows data from the same gel with ultrasound under the same conditions. There is no discernable difference in the mean velocity measured with and without ultrasound in these cases. In fact it is possible that an average velocity shift occurs in the data collected without ultrasound, which should not be the case. Too few cases were available in which data could be measured from a phantom to do deeper analysis. Comparing to data measured using the humidifier, which has a definitive shift in the mean velocity, it seems that no movement is present as a result of ultrasound application.

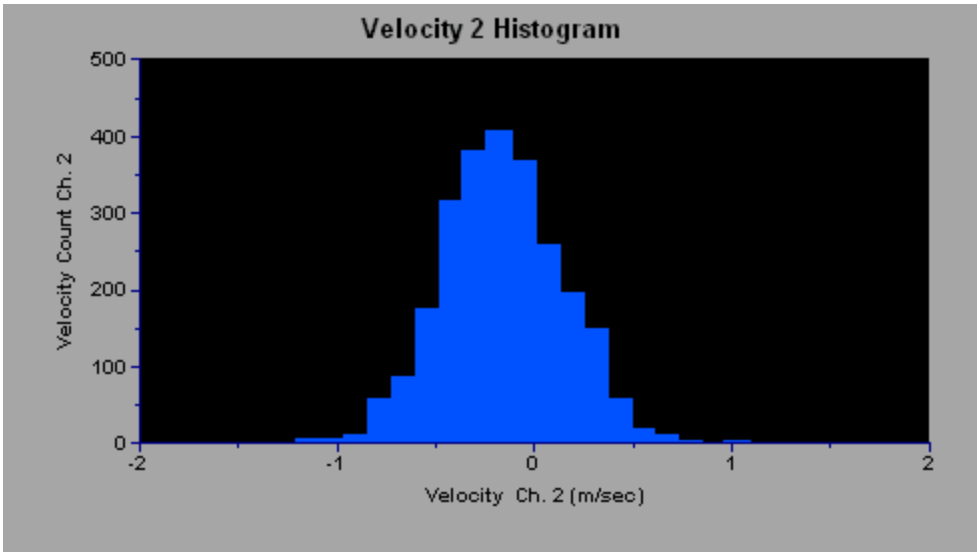

Figure 6 – Velocity data recorded from a gelatin phantom without ultrasound present.

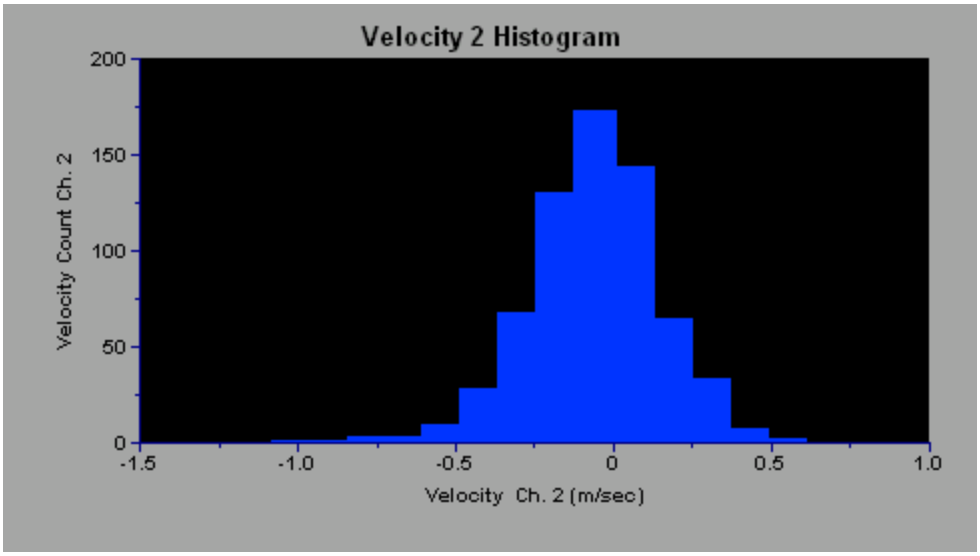

Figure 7 – Velocity data recorded from the same gelatin phantom as Figure 6, during ultrasound application.

Discussion and Conclusions

We performed experiments initially using alginate phantoms as tissue a mimicking material. Due to the relative opacity of this material when cured, optical absorption and scattering were too high in the material to allow for any realistic light penetration. It is likely the light became diffuse too quickly for coherent waveforms to be collected from scattered photons. The LDV system could not detect any data from the alginate phantoms, even if the measurement focus was placed at the surface of the phantom. In an attempt to improve the ability of the LDV system to detect a sufficient amount of light to enable measurement, phantom material was switched to clear setting gelatin. 22 um aluminum oxide particles were still used as scattering agents and as a detection base for the LDV system. Phantom design proceeded through several different iterations while attempting to generate a procedure robust enough for measurement.

In the first alginate phantoms the scattering region was placed 1.75 cm from the edge of optical incidence. This was intended to maximize ultrasound induced movement because the direction of ultrasound propagation could be aligned parallel to a measurement direction. Due to a lack of signal fidelity, the target scattering region was moved as close to the edge of optical incidence as possible (1-2mm). Due to physical limitation of the transducer size, this required the ultrasound to intersect the optical path at a 45° angle, reducing the component of ultrasound induced movement in the measurable direction. Again no receivable signal could be detected. Lastly a sheet of target scattering gel with a thickness 2-3mm was adhered to the optically incident face. Still no reliable signal could be detected. Concentrations of Al_2O_3 ranging from .1% by mass to 2% by mass were tested. 2% Al_2O_3 by mass generated nearly opaque target regions so higher concentrations were not considered. These same designs were considered using clear gelatin phantoms, but a detectable signal was too inconsistent to make measurements. If the system received any signal, it was most often suspected noise as shown in results figures 3 and 4. In the rare instance signal could be detected, no ultrasound effect could be observed.

Acoustic radiation force (ARF) and its effect on different tissues has been well documented over the course of more than 30 years [11][12]. Based on the designs of other acoustic RFP systems, it is extremely unlikely that insufficient force was being generated to induce tissue motion. As a result, it is most likely an issue with the LDV system in this context or compounding issues in the experimental setup. Several factors that may have contributed to or caused the lack of signal strength are discussed below.

The LDV system requires that the sample face be perpendicular to the path of optical incidence to prevent refraction of the beams and distortion of the focal region. While this was aligned

very closely using the portion of the beams reflected from the sample surface, it is possible small deviations reduced the ability for photons to be collected. Inhomogeneity's in the surface flatness of the sample could also contribute to non-perpendicular intersection and beam refraction. If either beam in a measurement pair are refracted differently from the other upon entering the sample, the focal region may not generate a recognizable fringe pattern, preventing any measurements. Extreme care was taken when constructing the phantoms to ensure the optically incident edge remained as flat as the glass mold, but aberrations were possible.

Aluminum oxide (Al_2O_3) particles with an average diameter of 22 um were used as seed particles for the LDV system. The refractive index of Al_2O_3 is 1.76 and the density is 3.95 g/cm^3 [13]. These properties are within the range of seed particles recommended by TSI for their LDV systems, indicating that Al_2O_3 should function with their system. Regardless, Al_2O_3 was not included in the suggested seed particle list. This particle choice may have contributed to the lack of detectable signal.

Most optical systems used in measuring non-superficial tissue properties use near infrared light with wavelengths exceeding 900 nm to increase penetration in tissue. The LDV system employed here uses 488 nm and 514.5 nm light. It may be that optical attenuation at these frequencies is too great for a relevant amount of light to be recovered from the phantom. We anticipated that using clear gelatin sample material would sufficiently compensate for this effect.

Gelatin based sample material was designed at concentrations such that sample sound speeds were near that of water (1500 m/s) [10]. If differences in sound speed between water and the sample existed, some refraction of the ultrasound waves would have occurred, changing the focal location. While this was controlled in sample design, when considered in conjunction with any optical refraction occurring at the laser entry point, it is possible that the ultrasound and LDV focal zones never overlapped. The ultrasound focus was scanned around the expected intersection location using the 2D motion stage to address this possibility.

During the course of experimentation with the LDV system, laser power dropped by nearly a factor of 2 in each beam (3.5 mW to 1.3 mW). The laser alignment was retuned, but original power could not be restored. Our collaborator managing the laser equipment indicated that this should not be an issue. The PMT voltages were increased to compensate for the drop in laser power. It is likely that in conjunction with the lossy sample material, the drop in laser power contributed to a lack of usable signal.

Despite our efforts, a procedure could not be developed in which the LDV system reliably collected any data from a tissue mimicking material. As a result, development of a device for

measurement of cerebral blood oxygenation and perfusion was postponed. This project may be started again at a later date if laser equipment in the near infrared range becomes available. Measuring fractional blood oxygenation and cerebral profusion directly and non-invasively would provide the best solution for monitoring resuscitation effectiveness. A functional device could be deployed in a large range of scenarios from the operating room to emergency medicine and would provide physicians with necessary feedback about patient cerebral health. Due to the difficulties associated with this project, my research focus shifted 6 months into my one year program. Still addressing resuscitation, my work refocused on the validation and design of an ultrasound based sensor to monitor blood flow in the carotid artery as an indication of cerebral profusion.

Development of a Carotid Artery Blood Flow Sensor

Introduction

Measuring cerebral oxygenation invasively or non-invasively currently requires specialized equipment that is limited to a hospital surgical setting [14]. In regard to resuscitation, this means the equipment to provide physicians or emergency medical staff with critical information regarding the neurological health of their patients is often inaccessible. While automated CPR machines, portable ventilators, and emergency defibrillators are available, there is little technology on the market that gives real time feedback concerning cerebral blood flow during emergency resuscitation, especially outside of an operating room. Ultrasound technology has been used in a wide variety of hemodynamic monitoring situations and has the potential for both low cost and portable devices. Doppler ultrasound techniques have been well developed and provide the ability to measure blood flow parameters non-invasively and in real time.

As the primary cerebral blood supply, measuring blood flow through the common carotid artery could be indicative of cerebral profusion. The carotid is easily accessible with ultrasound, lying only 1.5-2 cm below the surface of the skin. This provides an excellent target for monitoring during emergency situations where time is critical and setup needs to be exceedingly simple.

We propose developing an ultrasound based device for use in detecting blood flow through the common carotid artery as an indication of cerebral profusion. A functional end product would provide real time feedback concerning carotid blood flow, be portable, and simple to operate. My research into the development of this device has been divided into two primary phases. First, proof of concept experiments were necessary to determine whether ultrasound could reliably measure blood flow in the carotid artery under the extreme hemodynamic conditions present during resuscitation. To enable simple application while providing robust

measurements, a custom ultrasound device was needed. Second, I worked to develop a feasible transducer design to enable further research and device development.

Ethics Statement

All animal procedures were approved by the University of Washington Institutional Animal care and Use Committee (IACUC).

Methods: Proof of Concept Studies

In order to gather initial project feasibility data, it was necessary to evaluate the ability of a small, portable, non-imaging ultrasound transducer to detect blood flow over a range of hemodynamic conditions using our hardware system. Initial concept testing was performed in collaboration with Dr. Nathan White at Harborview Medical center. Dr. White's group was working with a poly-trauma pig model to develop drug and small molecule cocktails to improve trauma survival rates. During the course of their model, the pig sustains 4 traumatic injuries that include significant blood loss. This situation was ideal to monitor hemodynamic conditions from healthy to near death, ensuring device testing under extreme conditions. Initial data was collected from two animals. Our group was not involved in any set-up, animal monitoring, or surgical procedure and animal trails were performed under Dr. White's approved IACUC protocol. An overview of the poly-trauma model is presented below in order to lend context to the ultrasound data (Figure 8).

Animals were sedated using isoflurane and an automated ventilation system to minimize any possible discomfort. Standard medical monitoring equipment was utilized to track animal vitals (blood pressure, heart rate, body temperature, etc.). After sedation, the right femoral artery was catheterized to enable controlled bleeding at the onset of "trauma". An incision was made in the abdomen to allow access to the descending aorta and the spleen. The spleen was removed to prevent red blood cell infusion after trauma initiation and a wire was stitched through the descending aorta to later create a controlled aortic tear. The incision was stitched closed and the animal was monitored for 30 minutes to allow hemodynamic and vital equilibration. After equilibration, the right femur was fractured and a controlled traumatic brain injury (TBI) was induced. This marked the beginning of trauma and bleeds were initiated from the femoral catheterization and the aortic tear. After a 5 minute untreated trauma period, the research cocktail was administered over 10 minutes. The animal was monitored closely for 30 minutes, and a second infusion was given, again over the course of 10 minutes. The animal was then monitored for up to 6 hours or until death to assess the effectiveness of the infusion.

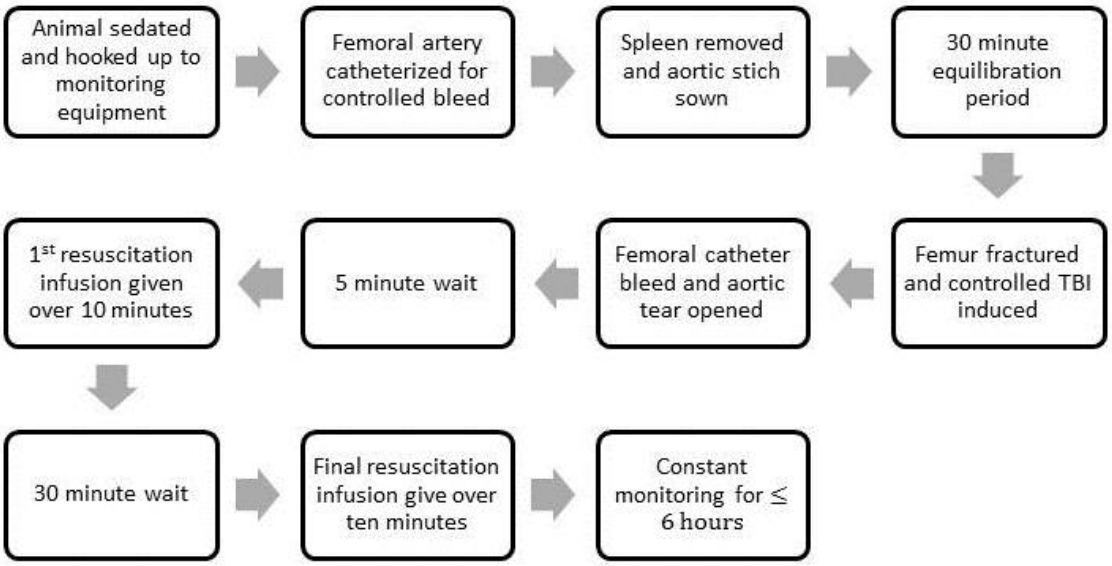

Figure 8 – A flow chart describing the steps taken in our collaborators pig experiments in order to lend context to ultrasound date. As soon as bleeds were initiated, we began recording ultrasound data.

In experiment number 1, blood flow data was collected from the left carotid artery using a 5 MHz, .5mm in diameter, single element ultrasound probe. Data was taken every 2 minutes during each infusion and every 5 minutes otherwise. Hemodynamic parameters changed rapidly during the drug infusion, necessitating more regular recordings. Heart rate and mean arterial pressure (MAP) were recorded at the beginning of each ultrasound data acquisition period. Blood flow data was unable to be collected prior to injury during the equilibration time due to inaccessibility of the carotid artery in the experimental setup at this point. In experiment number 2, the animal had inadequate collateral circulation around the femoral catheterization, causing insufficient blood flow to the leg. As a result, the animal was not a candidate for infusion testing per the above procedure. In order to allow carotid blood flow data to be collected, the aortic tear and femoral catheterization were opened and allowed to bleed without intervention. Ultrasound data was collected before the bleeds were induced and continuously from the induction of bleeding until it was necessary to euthanize the animal.

Ultrasound equipment used to monitor blood flow consisted of a Hokanson CP-1B Doppler Ultrasound Pulsing unit (Hokanson Inc., Issaquah WA), connected to a computer via an AlazarTech ATS460 analog to digital converter (Alazar Technologies, Pointe-Claire Quebec, Canada). Ultrasound was generated and received by a circular, single element, 5MHz, 5 mm in diameter transducer. The pulsing unit operates at a center frequency of 5.185 MHz, using

short, 3 cycle pulses at a pulse repetition frequency (PRF) of either 8 or 16 kHz. Data collected in the two experiments presented was obtained using a PRF of 8 kHz. 25 V_{pp} was applied to the transducer, producing intensities well under the diagnostic limit of .72 W/cm^2 I_{SPTA}. The pulsing unit performs quadrature demodulation on the analog signal prior to digitization. The Hokanson unit has a built in speaker that plays the Doppler signal as audio to allow easy blood flow detection. A built in range gate allows the depth at which Doppler signal is being detected to be modified. For each experiment, the range gate was set at 15mm which maximized the Doppler signal.

Data was collected and interpreted using a Matlab program which had been developed for a prior project that interfaced with Alazar ATS460 digitizer, allowing demodulated RF data to be read into Matlab. Data was sampled at 5.185 MHz and stored in 64 sample A-lines, centered at the range gate specified on the Hokanson pulsing unit. This corresponds to about 19mm in space, meaning only ultrasound data from inside the carotid was recorded. This increases efficiency and decreases noise as data from outside the area of interest is not present.

To review the data, a high pass wall filter was applied to remove tissue motion components and the filtered data was Fourier transformed. The data was multiplied by its complex conjugate to remove imaginary component, leaving only magnitude. The 64 depth samples were averaged together to eliminate noise. Doppler frequency information was converted to velocity and graphed over time. The visualization script can be viewed in the appendix.

Results and Conclusions

The aim of this study was to obtain data that demonstrated our systems ability to detect blood flow in the carotid artery across a range of hemodynamic conditions. With this in mind, five segments of data were selected from both pigs which span a large range of mean arterial pressures (MAP) and heart rates (HR) (Figures 9-13). Each graph shows detected blood velocity on the y-axis, and time on the x-axis. The image color represents normalized detected power at a given velocity with dark blue as 0 and red as 1. Power can be affected by several factors including blood hematocrit and wall filter design. The value of the detected power is not important to the determination of whether blood flow signals can be reliably detected so has been normalized to 1. A single cardiac cycle consists of systolic and diastolic phases where pressure and velocity alternate between high and low values respectively. Distinct cardiac cycles can be seen in Figures 9-13 following this pattern. HR in beats per minute was estimated from the ultrasound data by multiplying the number of systolic velocity peaks in 10 second interval by 6. Estimated HR for each figure is displayed in Table 2.

Measured MAP mmHg	Measured HR (BPM)	Estimated HR (BPM)	Figure #
72	207	204	9
73	127	126	10
56	140	138	11
41	157	156	12
28	182	180	13

Table 2 – Mean arterial pressure, measured heart rate, and estimated heart rate for each data set evaluated here.

Heart rates estimated from ultrasound data are within ± 3 beats per minute of data collected using the clinical life support equipment. This variance can be attributed to counting errors due to having an incomplete minute of data. Heart rate was accurately determined covering a range from over 200 BPM to 127 BPM. Blood flow was reliably detectable in all collected data from MAPs of 73 mmHg to as low as 28mmHg. Data outside of this range was not available within the confines of this experimental model. Of note, it appears that the relative power of the Doppler signal decreases in Figures 12 and 13 at MAPs of 41 and 28 mmHg respectively. This is especially apparent in figure 13 at a MAP of 28 mmHg. These data segments were taken during the second animal study where bleeding was induced and no additional fluids were given. This resulted in a dramatic decrease in blood volume and hematocrit. Since the Doppler signal is generated primarily via ultrasound interaction with red blood cells, the effective cross-sectional area scattering ultrasound was dramatically reduced. Additionally, at MAP values of 48 and 28 mmHg, peak systolic velocity and average velocity appear to decrease. Significantly decreased blood volume resulting in very low MAPs decreases the velocity at which blood travels. However, the ultrasound transducer used here was situated by hand over the carotid, introducing significant variability into the angle at which the ultrasound beam was aimed. Because the recorded blood velocity is dependent of the angle of incidence of the ultrasound beam, absolute velocity measurements were not reliable in these experiments. The transducer angle in all data was estimated to be 45° relative to the carotid artery and velocities were estimated using this value for visualization.

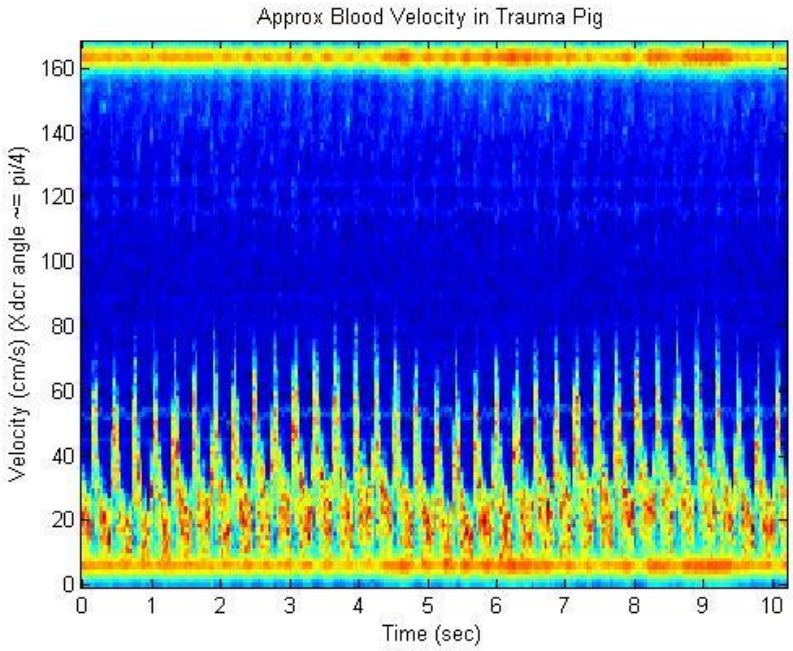

Figure 9 – Ultrasound Doppler data recorded at a MAP of 72 mmHg and a heart rate of 207 beats per minute.

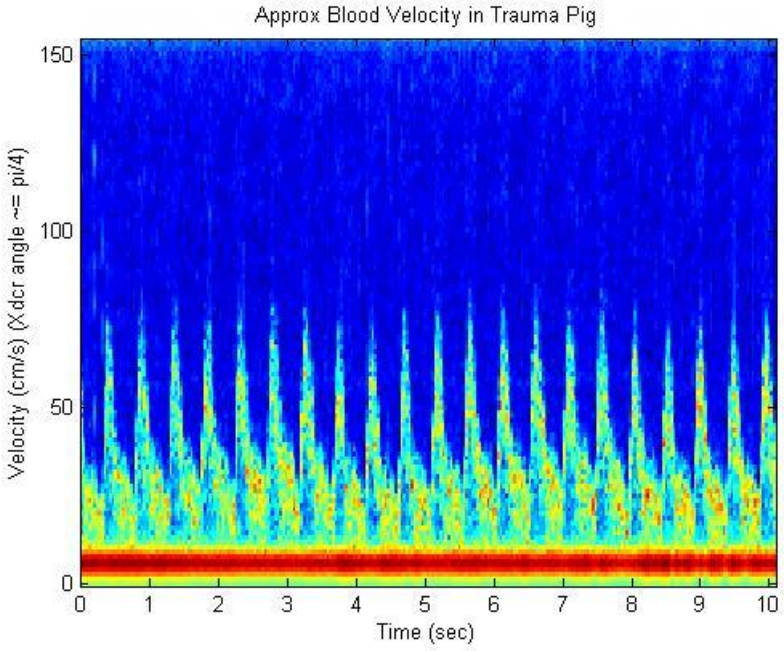

Figure 10 – Ultrasound Doppler data recorded at a MAP of 73 mmHg and a heart rate of 127 beats per minute.

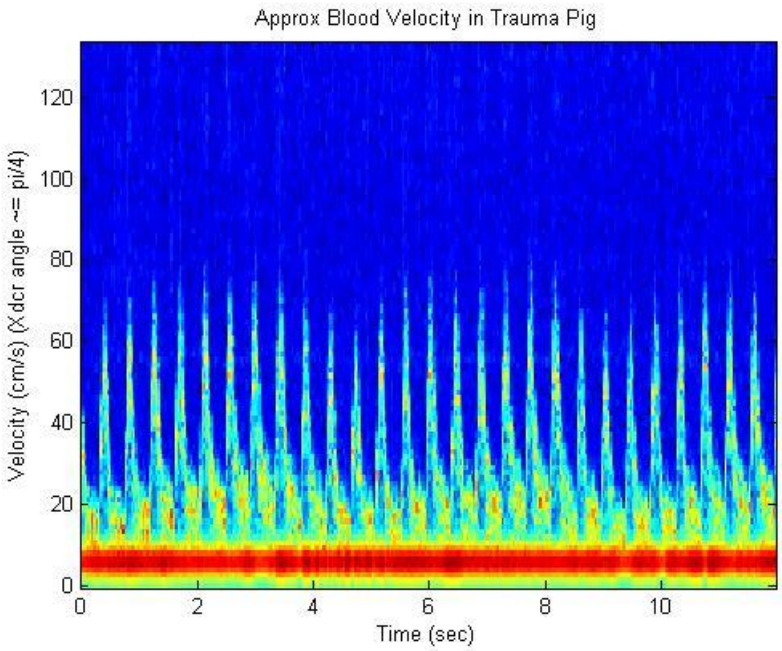

Figure 11 – Ultrasound Doppler data recorded at a MAP of 56 mmHg and a heart rate of 140 beats per minute.

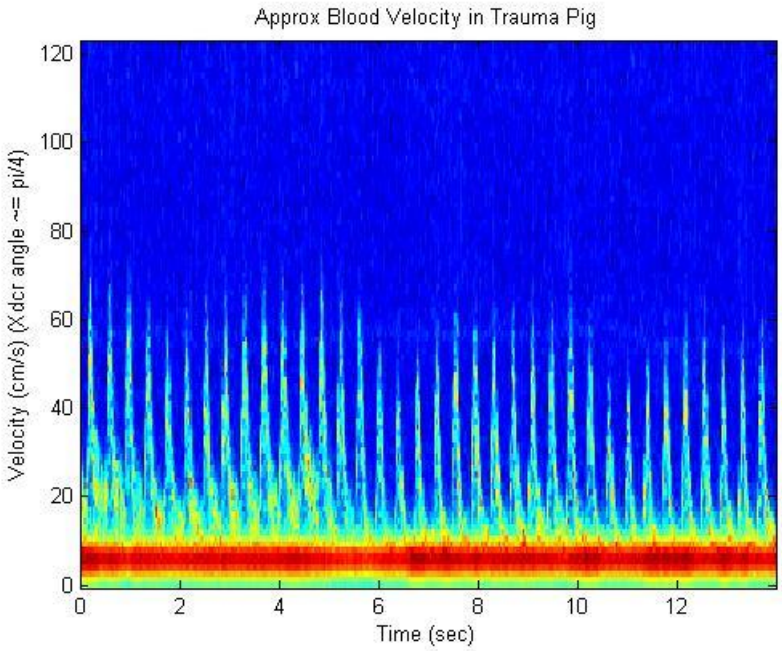

Figure 12 – Ultrasound Doppler data recorded at a MAP of 41 mmHg and a heart rate of 157 beats per minute.

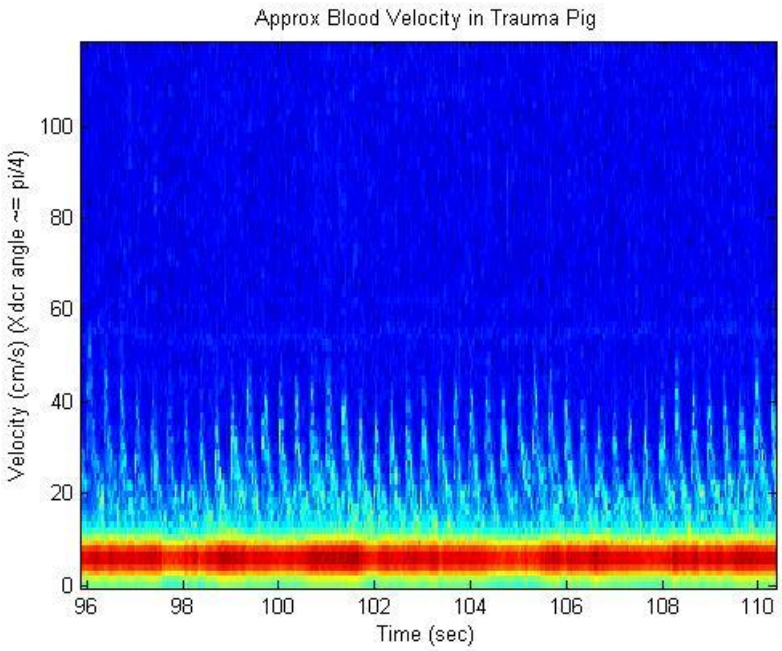

Figure 13 - Ultrasound Doppler data recorded at a MAP of 28 mmHg and a heart rate of 182 beats per minute.

Discussion

The ultrasound system tested here was able to reliably detect blood flow in the common carotid artery of two pigs undergoing resuscitation in a poly-trauma model. Animals in this model experienced a wide range of hemodynamic conditions as a result of significant blood loss, fluid reinfusion, and injury. Conditions present here represent the extreme end of likely resuscitation scenarios, though military trauma or severe automobile accidents could cause a similar extent of injury. The consistent ability of the ultrasound monitoring system tested here to make measurements reflects positively on the future of this technology and warrants further system development.

Despite the positive results, several study and system limitations were present that could negatively affect future performance. Because the ultrasound transducer in this system was handheld and the angle of incidence was variable, the magnitudes of velocity measurements were not reliable. A means to control transducer angle is necessary to provide accurate measurements. Additionally, the small size and angular sensitivity of the 5mm outer diameter, 5 MHz transducer make the device difficult to align and sensitive to any movement. This is not ideal as chest compression during resuscitation causes significant physical disturbance and an operator with ultrasound knowledge is necessary to use the device. A transducer setup designed specifically for this system could improve the robustness of measurement to physical disturbance and control device angle to enable consistent velocity information.

Doppler signal strength was significantly decreased when MAP fell to 28 mmHg. While still detectable, further decrease in red blood cell concentration or MAP could result an inability to detect blood flow. Information regarding the state the animal's blood relevant to acoustic properties was not available during these studies. Tracking blood hematocrit in the future may enable a correlation between ultrasound signal strength and a patient's blood properties. This could provide an additional source of information for attending medical personnel. Additional experimentation is also necessary to determine the threshold for complete signal loss and whether this could be reached before death.

Transducer design

Single element transducers can be made extremely small and portable, but have a relatively narrow natural focal field. The full width half max (FWHM) of a circular piston transducer can be estimated by calculating the beam divergence angle and adding the beam spread at the focus to the transducer diameter. The divergence angle can be calculated by

$$\theta = \sin^{-1}\left(\frac{1.2 * c}{D * f_0}\right) \qquad \text{Equation 1}$$

Where c is the speed of sound, D is the transducer diameter, and f_0 is the center frequency. Using equation 1, the FWHM beam diameter at the natural focus of the 5 mm outer diameter, 5MHz transducer used above is 5.3 mm. This results in the FWHM focal field covering only 13°. The common carotid artery lumen diameter ranges from 4.3-7 mm in healthy adults [15]. Small deviations in angle could easily place the majority of the ultrasound beam outside the target vessel, resulting in limited or no signal detection. In order improve our ultrasound systems ability to easily and accurately detect blood flow, a new transducer design was necessary.

The transducer must be compatible with existing equipment to facilitate further testing. The Hokanson pulsing unit uses a 3 cycle pulse width, 8 or 16 kHz selectable pulse repetition frequency, and operates at a center frequency of 5.185 MHz. These parameters are fixed and must be designed around. Additionally, the Hokanson unit has only a single channel of output, so multiplexed transducer designs are not possible. The output wattage of the pulsing unit is also limited; however, because this is model has not been in production for many years, specifications are not available. As the surface area of the piezoelectric elements increases, the necessary wattage to maintain 25 V_{pp} output increases. Care must be taken during design when considering multi-element designs to ensure that sufficient intensities are generated to produce reliable signal. Here 4 elements were selected to span 2 cm of the neck, allowing easy placement and balancing power demands. Further testing of the transducer will occur to determine if it is being driven at adequate intensities.

To reduce the need for device aiming and a knowledgeable operator, a design that allows the transducer to simply be placed on the neck over the carotid artery is ideal. To maximize the chance that the carotid artery is in the ultrasound path, multiple elements in a line configuration were selected as mentioned above. Circular elements were selected because they produce predicable beam patterns and are readily available for order. Element size was determined based the average depth of the carotid and natural focus of circular elements. The far field transition distance (natural focus) for a single circular element piston transducer is the ratio of the square of the diameter D to 4 times the wavelength λ (Eqn. 2).

$$Far\ Field\ Transition\ Distance = \frac{D^2}{4\lambda} \qquad \text{Equation 2}$$

The Hokanson pulsing unit in use for these studies operates at 5.185 MHz. This fixes the wavelength to c/f_0 (.297 mm). After consulting a collaborating emergency medical physician, it was determined that the average carotid artery depth is between 1.5 and 1.8 cm below the surface of the neck. Solving for the diameter of the transducer to place the natural focus at 1.8 centimeters, a transducer diameter of 4.6 mm is ideal. Simulations were performed in Matlab to evaluate the ultrasound field for single elements of different diameters at the required frequency (Figure 14-16). Diameters of 4 , 5, and 6 mm were evaluated in Figure 14, 15, and 16 respectively. The axial pressure line (top) and cross section of the ultrasound field (bottom) were calculated by solving the Rayleigh integral for a circular aperture in a time invariant scenario.

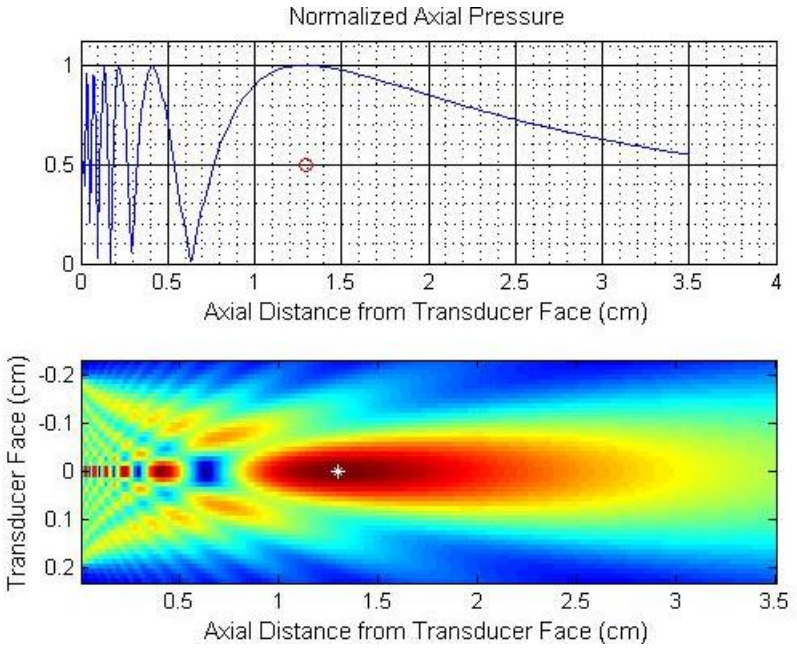

Figure 14 – Simulation of the axial pressure and a cross section through the ultrasound field of a 4 mm in diameter element. The point on each graph represents the calculated Rayleigh distance.

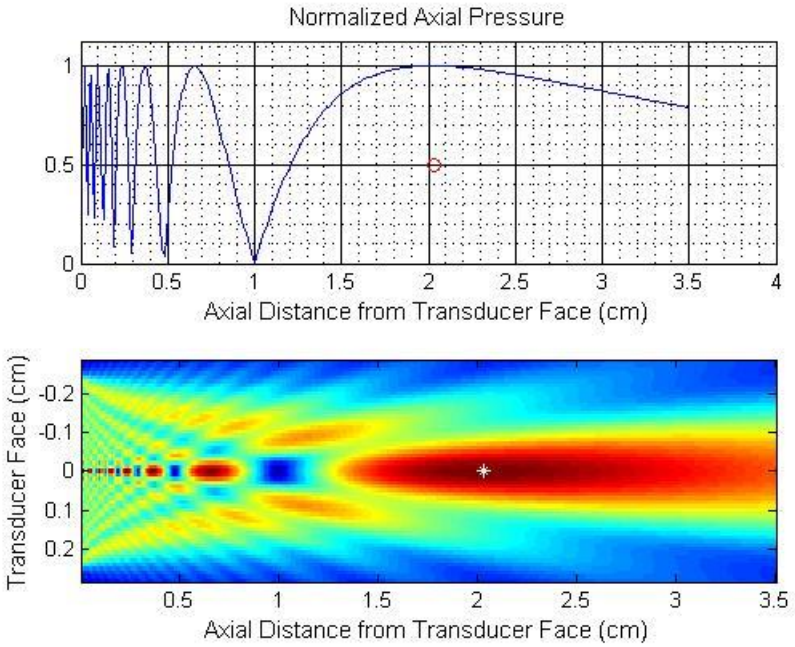

Figure 15 - Simulation of the axial pressure and a cross section through the ultrasound field of a 5 mm in diameter element. The point on each graph represents the calculated Rayleigh distance.

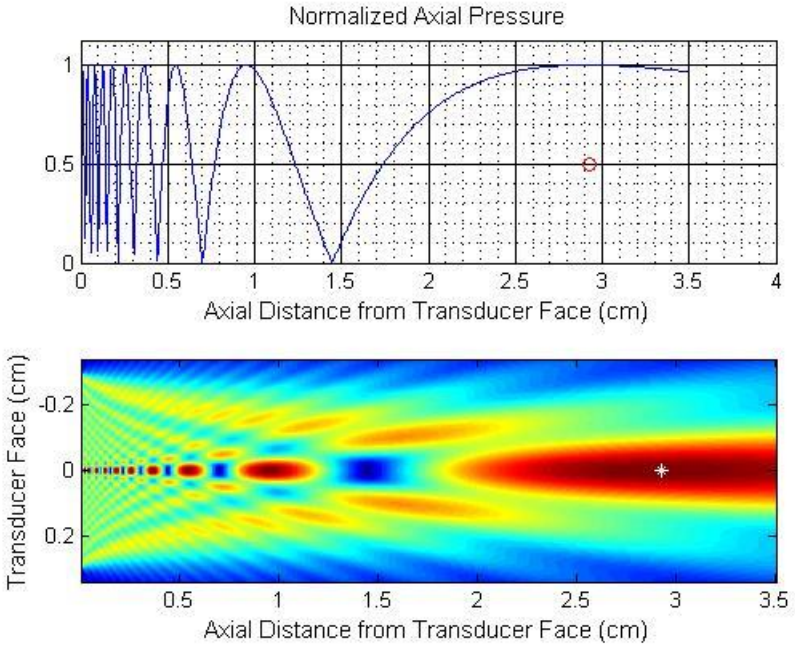

Figure 16 - Simulation of the axial pressure and a cross section through the ultrasound field of a 6 mm in diameter element. The point on each graph represents the calculated Rayleigh distance.

Numerous different piezoelectric materials exist for use in ultrasound applications. For Doppler ultrasound applications, broad-bandwidth devices (low quality factor) are necessary to allow for efficient detection of Doppler shifted signals that deviate from the device center frequency. Additionally, high coupling factors are desirable to improve energy transmission. These properties are available in soft PZT materials like Navy II or Navy IV. Navy type II material was selected for this application as it filled the above requirements and was readily available for order. Due to limitations in the readily available material, 5 mm in diameter, 5 MHz circular APC 850 (Navy type II) elements were purchased from American Piezo.

In order to achieve a broad bandwidth transducer that is capable of delivering sufficient energy to the target area, matching and backing layers must be carefully considered. The acoustic impedance, defined as the product of the density and speed of sound of material, is 33.5 Mrayl for the ceramic selected here. The acoustic impedance of water is 1.48 Mrayl. The reflected portion of an acoustic wave incident normally on a boundary is described by

$$R = \frac{Z_2 - Z_1}{Z_2 + Z_1} \qquad \text{Equation 3}$$

Where R is the reflection coefficient, Z_1 is the acoustic impedance of the current material, and Z_2 is the acoustic impedance of the destination material. It is apparent that the greater the difference in acoustic impedance, the less energy is transmitted from the piezoelectric element into the load material. It is valuable to minimize this difference in impedance using one or more matching layers that reduce the difference between layers to increase transmitted energy. Significant research has been done in optimizing matching layers for ultrasound devices. It has been shown that the ideal layer thickness is one quarter wavelength and the ideal impedance for a single matching layer is the geometric mean of the transducer (Z_1) and load (Z_3) impedances (Eqn. 4) [16]. For two matching layers, it has been shown that the ideal impedances should follow equations 4 and 5 for the 1st and 2nd layer respectively [17].

$$Z_m = \sqrt{Z_1 * Z_3} \qquad \text{Equation 3}$$

$$Z_{m1} = (Z_{load}^3 * Z_{source}^4)^{1/7} \qquad \text{Equation 4}$$

$$Z_{m2} = (Z_{load}^6 * Z_{source}^1)^{1/7} \qquad \text{Equation 5}$$

Backing layers are added to a transducer to damp any ring-down the element experiences after the driving waveform has been applied [17]. The material must be sufficiently attenuating to prevent reflections from the back wall of the backing layer. The backing layer ideally is closely matched to the piezoelectric element to prevent reflection from the interface between the layers. Common backing materials include tungsten-loaded epoxy, pyrolytic brass, and highly attenuating foams [18].

Simulations were performed using the PiezoCAD software package (Sonic Concepts Inc., Bothell WA) to determine the desired matching and backing layers. Simulations of the final design are shown here in Figures 17-19. Two matching layers, each one quarter wavelength thick, with impedances as described in equations 4 and 5 were selected to maximize energy transfer from the transducer. A 20 λ backing layer was selected to damp any ringing effects and to add structural stability to the device. Tungsten loaded epoxy was used for both the matching and backing layers. Its impedance was tuned by varying the amount of quantity of tungsten in the mixture as described by Bernassau et al [19]. The impedance of the backing material was set to the maximum acoustic impedance for this mixture is 8.9 Mrayl to match it as closely as possible to the element impedance.

Simulations represented the properties of a single element. Figure 17 shows the electrical impedance properties of the transducer. When driving multiple elements in parallel, the electrical impedance is the inverse of the sum of the inverses of the impedances for each element. The Hokanson pulsing unit drives a 50 ohm load. Matching the value as closely as possible while considering transmit efficiency and ringing is desired. It will be necessary to electrically match the system of four elements to the 50 ohm load at a later point for this design. Figure 18 shows the impulse response of the system after a 2 cycle, 5 MHz excitation pulse. The lack of ringing in the excitation waveform is ideal for broad bandwidth applications like Doppler ultrasound. Figure 19 shows the transmit efficiency of the device. At 310 mW/W, this was 3 times higher than the single matching layer, contributing significantly to the selection of this design.

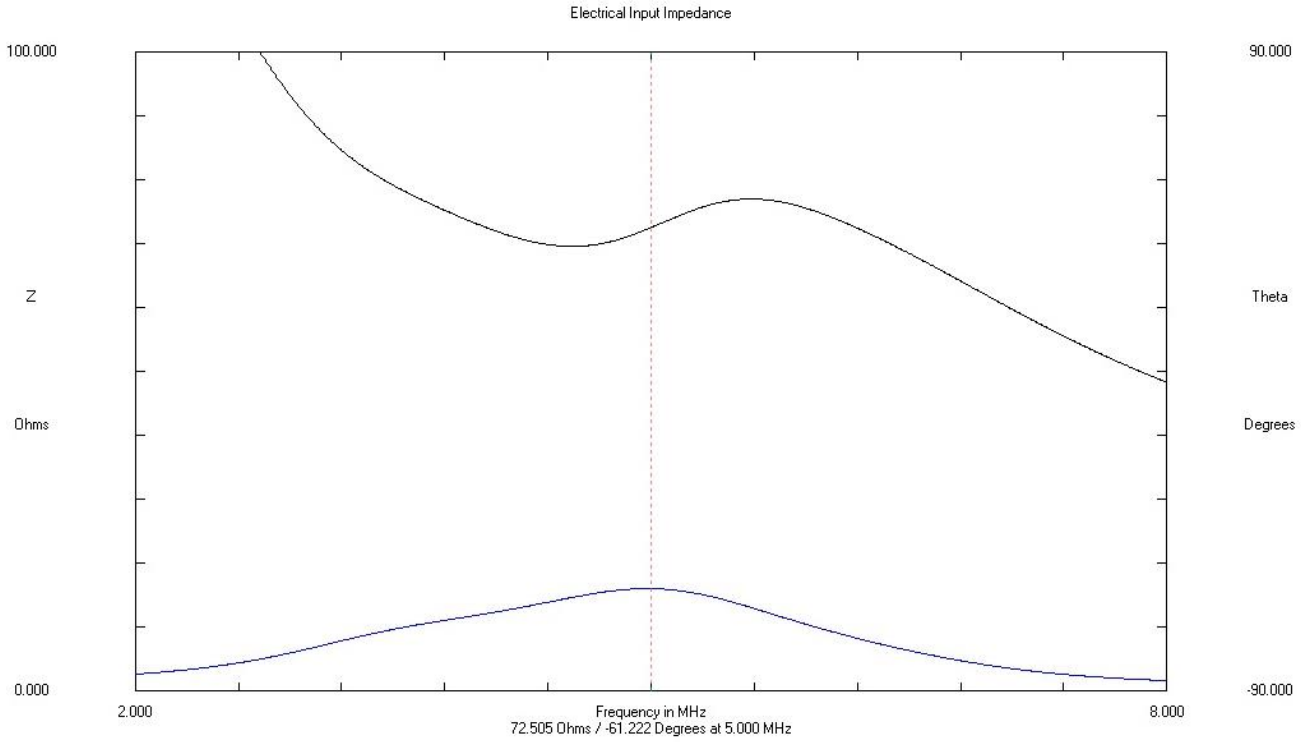

Figure 17 – PiezoCad simulation of the designed ultrasound transducer showing electrical impedance. At 5 MHz, the electrical impedance is 72.505 ohms and -61.222 degrees.

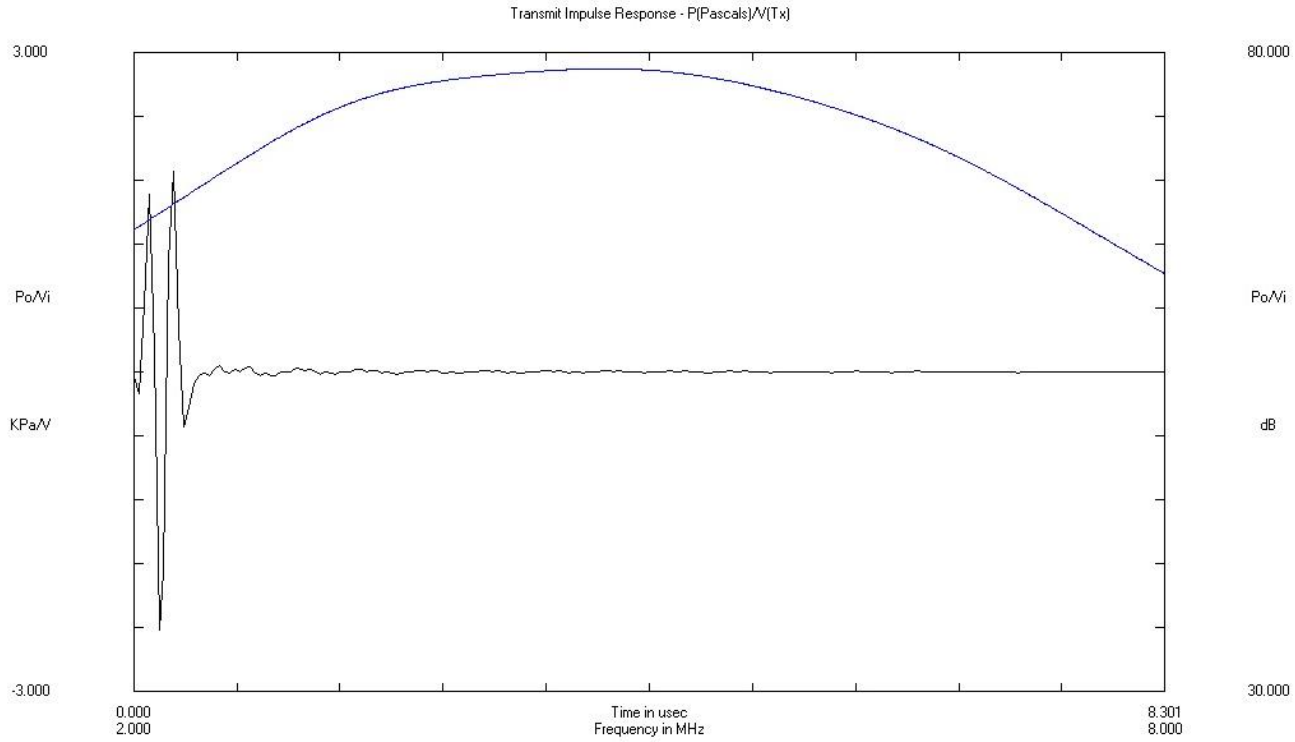

Figure 18 – PiezoCad simulation of the designed ultrasound transducer showing impulse response to at 2 cycle, 5MHz input waveform.

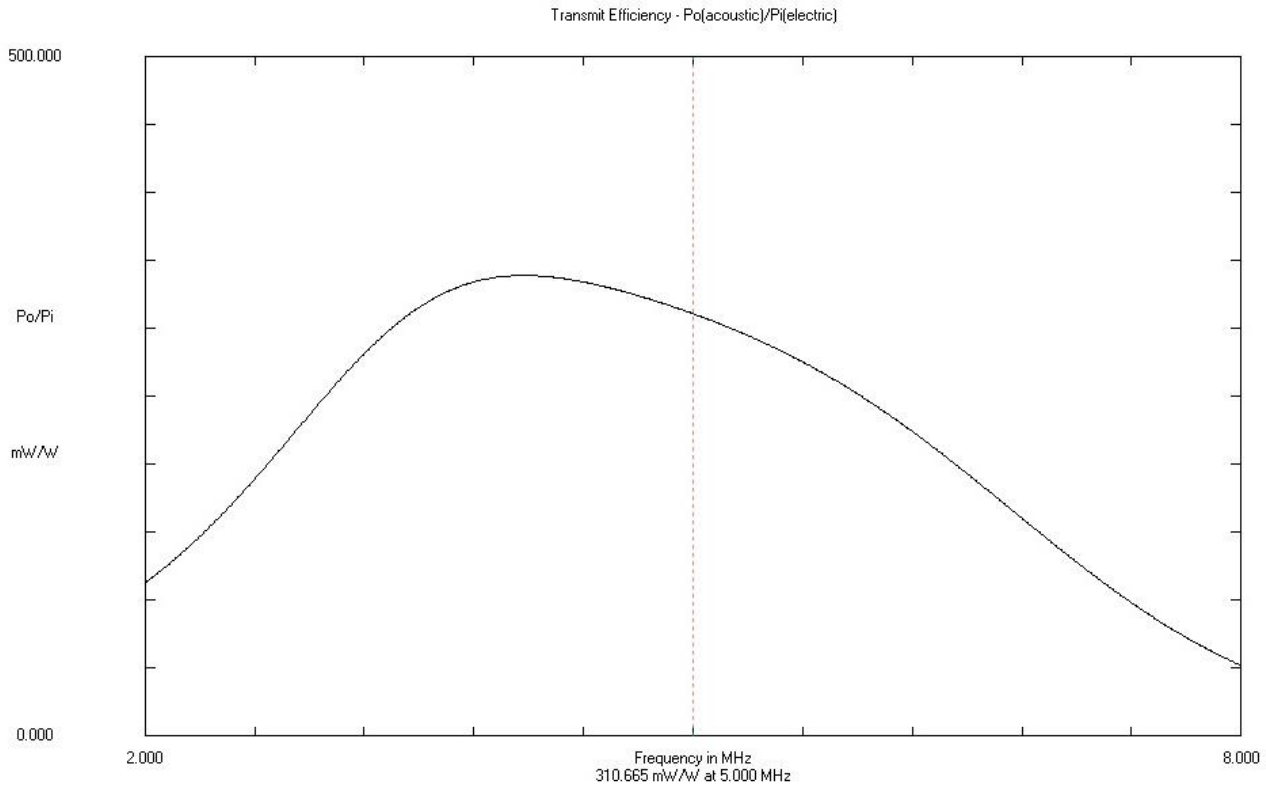

Figure 19 - – PiezoCad simulation of the designed ultrasound transducer showing transmit efficiency. At 5 MHz, the transmit efficiency is 310.665 mW/W.

After analyzing transducer simulations for one and two matching layer and various backing layer designs, a two matching layer, 20 wavelength thick backing layer configuration was selected (Figure 20). Utilizing two matching layers increased the transducer transmit efficiency to near 30% (310mW/W) without an electrical matching network. Additionally, reducing the impedance barrier between the piezoelectric element and the load with two matching layers can improve sensitivity to received signal by reducing the percentage of the signal that is reflected. A 20 wavelength backing layer was selected to reduce ringing, increase bandwidth, and provide structural stability for the very thin element/matching layer assembly. Due to material limitations, the backing layer impedance was set to 8.86 MRayl. This is the maximum possible impedance using a tungsten loaded epoxy. The final transducer design (Figure 21) houses the four elements in a high precision 3D printed case. The case includes a 30° angle on the ultrasound incident face to ensure that velocity measurements are accurate. The assembly is designed to be taped over the carotid artery, making the device resilient to physical disturbance.

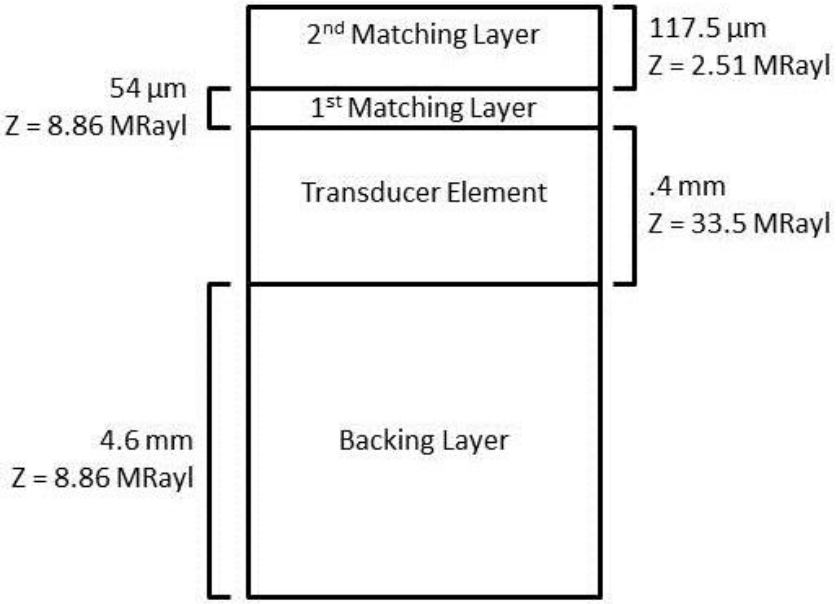

Figure 20 – Transducer element assembly schematic

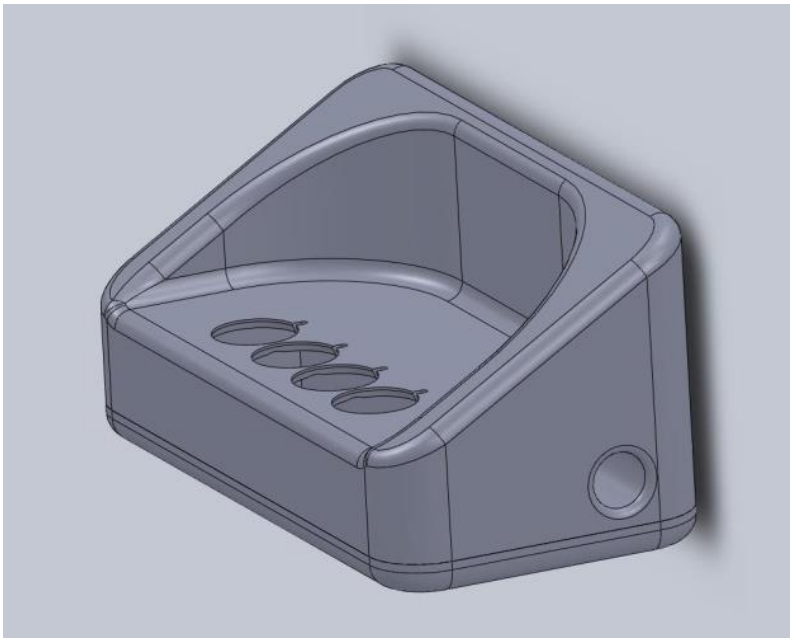

Figure 21 – Final design for the transducer housing.

Acknowledgements

I would first and foremost like to thank my PI, Dr. Pierre D. Mourad for his continued support and mentoring over the course of a tumultuous project. Thank you to Dr. Nathan White for allowing enabling the collaboration on such a relevant animal model. We are grateful for the collaboration and help of Dr. Bill Asher who let us use LDV equipment and lab space for experiments and Dr. Hassan Arbab actively collaborated with us in an attempt to get the LDV system working. Brain MacConaghy and Adam Maxwell provided invaluable support and mentoring during the design of a new transducer system. John Kucewicz designed the code to interface with the Alazar digitizer and provided significant technical support for all things code related. Lastly, thanks to Abbi McClintic who provided logistical support for the running of this project, without whom our lab might not function.

Citations

[1] Alan S. Go, MD, et al. Heart Disease and Stroke Statistics – 2013 Update. American Heart Association Statistics Committee and Stroke Statistics Subcommittee. *Circulation*, 2013; 127:000-000.

[2] Neumar RW, Nolan JP, Adrie C, Aibiki M, Berg RA, et al. Post–Cardiac Arrest Syndrome. Epidemiology, Pathophysiology, Treatment, and Prognostication A Consensus Statement From the International Liaison Committee on Resuscitation (American Heart Association, Australian and New Zealand Council on Resuscitation, European Resuscitation Council, Heart and Stroke Foundation of Canada, InterAmerican Heart Foundation, Resuscitation Council of Asia, and the Resuscitation Council of Southern Africa); the American Heart Association Emergency Cardiovascular Care Committee; the Council on Cardiovascular Surgery and Anesthesia; the Council on Cardiopulmonary, Perioperative, and Critical Care; the Council on Clinical Cardiology; and the Stroke Council. Circulation. 2008;118:2452–2483.

[3] Laura L. Dugan, Dennis W. Choi. Basic Neurochemistry: Molecular, Cellular and Medical Aspects. 6th Edition. Philadelphia: Lippincott-Raven; 1999.

[4] Ewy GA. Scand J Trauma Resusc Emerg Med. The cardiocerebral resuscitation protocol for treatment of out-of-hospital primary cardiac arrest. 2012 Sep 15;20:65. Doi: 10.1186/1757-7241-20-65.

[5] McCormick PW, Stewart M, Goetting MG, Dujovny M, Lewis G, Ausman. Noninvasive cerebral optical spectroscopy for monitoring cerebral oxygen delivery and hemodynamics. Crit Care Med 1991;19:89-97.

[6] J. M. Murkin and M. Arango. Near-infrared spectroscopy as an index of brain and tissue oxygenation. Br. J. Anaesth. (2009) 103 (suppl 1): i3-i13 doi:10.1093/bja/aep299

[7] Xiao Xu, Honglin Liu, Ligon V. Wang. Time-reversed ultrasonically encoded optical focusing into scattering media. Nature Photonics. 2011, January. DOI: 10.1038/NPHOTON.2010.306.

[8] Pierre Bouzat, Nathanlie Sala, Jean-Francois Payen, Mauro Oddo. Beyond intracranial pressure: optimization of cerebral blood flow, oxygen, and substrate delivery after traumatic brain injury. Annals Intensive Care. 2013. DOI: 10.1186/2110-5820-3-23.

[9] Matin O. Culjat, David Goldenberg, Priyamvada Tewari, Rahul S. Singh. A Review of Tissue Substitues for Ultrasound Imaging. Ultrasound Medicine and Biology. 2010. DOI:10.1016/j.ultrasmedbio.2010.02.012

[10] Jason R. Cook, Richard R. Bouchard, Stanislav Y. Emelianov. Tissue-mimicking phantoms for photoacoustic and ultrasonic imaging. Biomed Optics Express. 2011.

[11] Chu B-T and Apfel R. E. Acoustic radiation pressure produced by a beam of sound. J. Acoust. Soc. Am. 1982. 72 1673–87.

[12] Jiang, ZY. Greenleaf JF. Acoustic radiation pressure in a three-dimensional lossy medium. J. Acoust. Soc. Am. 1996. DOI:10.1121/1.416236

[13] Roger H. French, Harald Mullejans, David J. Jones. Properties of Aluminum Oxide: Determined from Vacuum Ultraviolet and Electron Energy-Loss Spectroscopies. J. Am. Ceram. Soc. 1998.

[14] Limbu YR, Gurung G, Malla R, Rajbhandari R, Regmi SR. Assessment of carotid artery dimensions by ultrasound in non-smoker healthy adults of both sexes. Nepal Med Coll J. 2006.

[15] Shung, K.K., Zippuro, M. Ultrasonic transducers and arrays. Engineering in Medicine and Biology Magazine, IEEE. 1996. DOI:10.1109/51.544509.

[16] Kinsler LE, Frey AR, Coppns AB, Sanders JV. Fundamentals of Acoustics, 3rd Ed. John Wiley, New York. 1982.

[17] Brown L.F. The Effects of Material selection for backing and wear protection/quarter-wave matching of piezoelectric polymer ultrasound transducers. Ultrasonics Symposium Proceedings. 2000.

[18] A.L. Bernassau, D. Hutson, C.E.M. Demore, S. Cochran. Characterisation of an Epoxy Filler for Piezocomposite Material Compatible with Microfabrication Processes. IEEE International Ultrasonics Symposium Proceedings. 2008.

Appendix

Script 1

```
%% Open .bin file

clc; clear all; close all;

%get file information from user
pathName = strcat(uigetdir,'\');
fileName = dir(strcat(pathName,'\ResusData*'));


for loop = 1:size(fileName,1);
%% read partial / full file
% [fileName,pathName] = uigetfile('ResusData*.bin');
fid = fopen([pathName,fileName(loop).name],'r');

fileVersion = fread(fid,1,'int32');
switch fileVersion
    case 1,
        fileTime = fread(fid,1,'double');
        inputRangeVolts = fread(fid,1,'double');
        samplesPerRecord = fread(fid,1,'int32');
        recordsPerBufferCollected = fread(fid,1,'int32');
        recordsPerBuffer = fread(fid,1,'int32');
        enableRecordHeaders = fread(fid,1,'int32');
    otherwise,
        error(sprintf('unknown file version ''%d''',fileVersion));
end

data = fread(fid,inf,'uint16');

fclose(fid);

if enableRecordHeaders  %Parse out header
    data = reshape(data,samplesPerRecord+8,[]);
    header = data(1:8,:);
    data = data(9:end,:);
else
    data = reshape(data,samplesPerRecord,[]);
    header = [];
end

data = (double(data)-2^15)/2^15*inputRangeVolts;    % Center and scale

%reshaped .bin data
data = complex(data(:,1:2:end),data(:,2:2:end));
data = reshape(data,samplesPerRecord,recordsPerBufferCollected,[]);



%% Plot
```

```
%Normal Human carotid artery flow velocity .2-1.7 m/s
%Sampling freq = 5.185

if loop == 1
    PRF = 8e3; %kHz
    f_0 = 5.185e6; % MHz
    c = 1540; % m/s
    numBuffers = 128;

    [bb,aa] = butter(3,.08,'high');  %Highpass Wallfilter (5th order
butterworth)
end

    %t = 304/PRF*max(size(data,3),numBuffers);  %for viewing smaller data
sections
    t = 304/PRF*size(data,3);  %time axis for entire data set

%Takes up to numbuffers of data from start of collection period (each 128
lines).
%Beginning of collection corresponds to time of HR&BP measurement

dTemp = data(:,:,:); %1:min(size(data,3),numBuffers));

[dOut, dFFTOut] =
QuickVisDisplay(dTemp,size(data),bb,aa,numBuffers,PRF,f_0,c,t); %filter and
disp

% if loop == size(fileName,1);    %displays last buffer of data collecte
%
%     dTemp = data(:,:,end-numBuffers+1:end);
%     [dOut, dFFTOut] =
QuickVisDisplay(dTemp,size(data),bb,aa,numBuffers,PRF,f_0,c,t);
%
% end



end
```

Script 2: Called function

```
%Filters and displays data into velocity m-mode.
%Takes in reshaped data to process, original reshaped data, filter coeffs,
number of buffers to process,
%system PRF, system center freq, medium sound speed, and total time

function [dTemp, dFFT] = QuickVisDisplay(dTemp, dataSize, bb, aa, numBuffers,
PRF, f_0, c, t)

dTemp = filter(bb,aa,dTemp,[],1);   %removes low freq components (fast time)
cutoff ->(1/2*samp_freq)*.125 =~ 1.25 MHz
dTemp = filter(bb,aa,dTemp,[],2);   %wall filter (slow time) cutoff -> 200 Hz
```

```
dTemp =
dTemp.*repmat(hanning(size(dTemp,2))',[size(dTemp,1),1,size(dTemp,3)]);
%applies windowing function in slow time (128 lines)

dFFT = fft(dTemp,[],2); %FFT across slow time
dFFT = dFFT.*conj(dFFT);   %take magnitude
dFFT = squeeze(mean(dFFT,1));   %average through depth

figure();   %plots velocity vs time
imagesc([0:1/(dataSize(3)-1):t], [0:PRF/2/(size(dTemp,2)-
1):(PRF/2)].*(c/f_0./cos(pi/4)).*100, 20*log10(dFFT)); %x,y,C
ylabel('Velocity (cm/s) (Xdcr angle ~= pi/4)'); xlabel('Time (sec)');
title('Approx Blood Velocity in Trauma Pig');
set(gca,'YDir','normal');

end
```